Front. Optoelectron. China 2011, 4(4): 448–453
DOI 10.1007/s12200-011-0189-y

REVIEW ARTICLE

6-channel photonic generation of ultra-wideband signals using multiple nonlinear characteristics in a parallel FOPA structure

Liang ZHAO (✉)[1], Junqiang SUN[2]

1 Wuhan Foreign Languages School, Wuhan 430022, China
2 Wuhan National Laboratory for Optoelectronics, College of Optoelectronics Science and Engineering, Huazhong University of Science and Technology, Wuhan 430074, China

Abstract We propose an approach to generating 6-channel polarity-inverted ultra-wideband (UWB) doublets by utilizing the parallel fiber-optical parametric amplifier (FOPA) configuration. The pulse-splitting effect in a highly nonlinear fiber (HNLF) is exploited to generate the double-overshoot and the double-undershoot, which are the basic components required to form a UWB pulse. Under the circumstances of different relative time advance/delays (RTADs) and different initial Gaussian pulse durations, the key parameters, including center frequency (Fc), 10-dB bandwidth (BW_{10dB}) and fractional bandwidth (FBW) for a UWB doublet are systematically investigated, eventually proved in line with the U. S. Federal Communications Commission (FCC) regulation.

Keywords ultra-wideband (UWB), pulse-splitting, fiber-optical-parametric-amplifier (FOPA), highly nonlinear fiber (HNLF)

1 Introduction

Ultra-wideband (UWB) has attracted more and more attentions for its wide applications in recent years, such as short-range high-throughout wireless communications and sensor networks [1]. The intrinsic property of UWB focuses on high-data-rate transmission, high capacity in space, immunity to multipath fading, extremely short-time duration, wide bandwidth and low power spectral density [2]. In light of these advantages, UWB has a potential to solve the contradiction between the request of high-rate Internet access and distribution of more and more crowded frequency resource. The definition of UWB is put forward by the Federal Communications Commission (FCC) regulation for indoor UWB systems with the frequency range covering from 3.1–10.6 GHz, and the UWB signal should have a 10-dB bandwidth (BW_{10dB}) of > 500 MHz or a fractional bandwidth (FBW) of $> 20\%$ [1].

Recently, more and more approaches to generating a UWB pulse have been reported [3–5]. Wang et al. proposed and demonstrated an approach to generating all-optical UWB monocycle pulses by exploiting the parametric attenuation effect of sum-frequency generation in a periodically poled lithium niobate waveguide [6]. Bolea et al. using an N tap microwave photonic filter theoretically proposed and experimentally confirmed a scheme for the higher-order UWB pulse generation, and the UWB generator could be adapted to different modulation formats with a reconfiguration time up to tens of nanoseconds by using optical devices available commercially [7]. A simple approach to generating UWB doublets by using the cross-gain modulation in a fiber-optical-parametric-amplifier (FOPA) configuration [8] evokes our attention, which was experimentally demonstrated by Li. Owing to both the gain-saturation and optical-parametrical-attenuation effects in a highly nonlinear fiber (HNLF), the pulse-splitting phenomenon [9], was proposed by Cao et al., which could be potentially utilized to form a double-overshoot or a double-undershoot for a UWB doublet. In terms of the above investigations, we ever proposed and demonstrated an approach to generating the single-channel UWB doublet by exploiting the nonlinearities in one piece of HNLF [10].

In this paper, we further propose a parallel FOPA structure to realize 6-channel polarity-inverted UWB doublets based on the scheme in Ref. [10], and the factors presumably influencing the characteristics of a UWB doublet, i.e., between the overshoot and the undershoot, as

Received August 30, 2011; accepted September 14, 2011

E-mail: liangshao_acool@smail.hust.edu.cn

well as pulse duration of the initial Gaussian signal, are investigated in detail. Moreover, the key parameters for a UWB doublet, including center frequency (Fc), BW_{10dB} and FBW, are also systematically investigated. At theend, we propose and discuss possible solutions to optimizing the UWB pulse, including the UWB-over-fiber technology.

2 Principal and analysis

HNLF is a promising candidate widely applied to various optical signal processing systems, especially for the microwave generation system [11]. Figure 1(a) schematically illustrates a HNLF-based parallel FOPA configuration, and the pump wave is modulated in phase by a pseudorandom bit sequences (PRBS) to suppress the stimulated Brillouin scattering. After that, two erbium doped fiber amplifiers (EDFAs) provide enough energy to the pump and signal, while the tunable band-pass filter (TBPF)1 is used to suppress the amplified simultaneous emission noise and select the pump wave. The signal wave is injected into the other route by tunable laser sources (TLS)2 and modulated in amplitude by amplitude modulator (AM). The pump and signal waves are then divided into two parts by OC1 and OC2, and are successively combined by OC3 and OC4. Afterwards, the pump and signal waves are launched into two different HNLFs respectively to realize the optical parametric process. Eventually, the two-route output waves (pump, signal, idler, and satellite) will be separated into eight parts by OCs and TBPFs, and variable optical attenuators (VOAs) together with optical delay lines (ODLs) are used to tune the amplitude and collimate the central location of the overshoot and the undershoot. Digital communications analyzer (DCA) and electrical spectrum analyzer (ESA) are utilized to monitor the temporal waveform and electrical spectrum of a UWB pulse, respectively. Note that, there are eight different waveforms located from port 1 to port 8. As illustrated in Fig. 1(b), when selecting a short-length fiber (i.e., HNLF1), the single-overshoot or the single-undershoot is available. In contrast, when selecting a relatively long-length fiber (i.e., HNLF2), the double-undershoot or the double-overshoot are formed. Through combining some specific ports, we can obtain 6-channel polarity-inverted UWB doublets, and UWB_{jk} (j = 1, 2, 3, 4 and k = 5, 6, 7, 8) is defined as a complex signal by combining the pulses at the j-th and the k-th ports, i.e., UWB_{16} is a positive UWB doublet obtained by connecting port 1 and port 6. In simulation, we choose the related parameters for the signal and pump waves, together with the HNLFs as follows: P_{10} = 0.64 mW, P_{20} = 900 mW, β_2 = 1.2 ps^2/km, $\beta_4 = 2\times10^{-5}$ ps^4/km, λ_1 = 1556.4 nm, λ_2 = 1550 nm, L_1 = 250 m (fiber length for HNLF1), L_2 = 450 m (fiber length for HNLF2), T_0 = 35 ps, γ = 0.017 /km/mW. The physical implication of all the above symbols can be referred to Ref. [10], and the basic coupled-wave nonlinear Schrödinger equations are expressed as [10]:

$$\begin{aligned}\frac{\partial A_1}{\partial z} = {} & \mathrm{i}\gamma\left[|A_1|^2 + 2\sum_{j(\neq 1)}|A_j|^2\right]A_1 \\ & + 2\mathrm{i}\gamma A_1^* A_2 A_3 \exp(\mathrm{i}\Delta\beta_1 z) \\ & + \mathrm{i}\gamma A_4^* A_2^2 \exp(-\mathrm{i}\Delta\beta_2 z) \\ & + 2\mathrm{i}\gamma A_2^* A_3 A_4 \exp(\mathrm{i}\Delta\beta_3 z), \end{aligned} \tag{1}$$

$$\begin{aligned}\frac{\partial A_2}{\partial z} = {} & \mathrm{i}\gamma\left[|A_2|^2 + 2\sum_{j(\neq 2)}|A_j|^2\right]A_2 \\ & + 2\mathrm{i}\gamma A_2^* A_1 A_4 \exp(\mathrm{i}\Delta\beta_2 z) \\ & + \mathrm{i}\gamma A_3^* A_1^2 \exp(-i\Delta\beta_1 z) \\ & + 2\mathrm{i}\gamma A_1^* A_3 A_4 \exp(\mathrm{i}\Delta\beta_3 z), \end{aligned} \tag{2}$$

$$\begin{aligned}\frac{\partial A_3}{\partial z} = {} & \mathrm{i}\gamma\left[|A_3|^2 + 2\sum_{j(\neq 3)}|A_j|^2\right]A_3 \\ & + 2\mathrm{i}\gamma A_4^* A_1 A_2 \exp(-\mathrm{i}\Delta\beta_3 z) \\ & + \mathrm{i}\gamma A_2^* A_1^2 \exp(-\mathrm{i}\Delta\beta_1 z), \end{aligned} \tag{3}$$

$$\begin{aligned}\frac{\partial A_4}{\partial z} = {} & \mathrm{i}\gamma\left[|A_4|^2 + 2\sum_{j(\neq 4)}|A_j|^2\right]A_4 \\ & + 2\mathrm{i}\gamma A_3^* A_1 A_2 \exp(-\mathrm{i}\Delta\beta_3 z) \\ & + \mathrm{i}\gamma A_1^* A_2^2 \exp(-\mathrm{i}\Delta\beta_2 z). \end{aligned} \tag{4}$$

Here, $\Delta\beta_k$ (k = 1, 2, 3) is the linear phase mismatch, and its analytical expressions can be referred to Refs. [12,13]. $A_j(t, z)$ (j = 1, 2, 3, 4) is the slowly varying complex amplitude of the electrical field of signal, pump, idler and satellite wave, respectively. In our case, we take into account higher-order FWM sidebands owing to high initial pump power and high-efficiency FWM. Remarkably, amplitudes of the Gaussian pulse signal and the continuous-wave (CW) pump are given by

$$A_1(t,0) = \sqrt{P_{10}}\exp(-t^2/2T_0^2),\ A_2(t,0) = \sqrt{P_{20}}. \tag{5}$$

It is worthy noting that P_{10} is the peak power of signal pulse at the input port of HNLF, while P_{20} is the CW pump power at the input port of HNLF.

The interesting phenomenon that, the signal pulse is

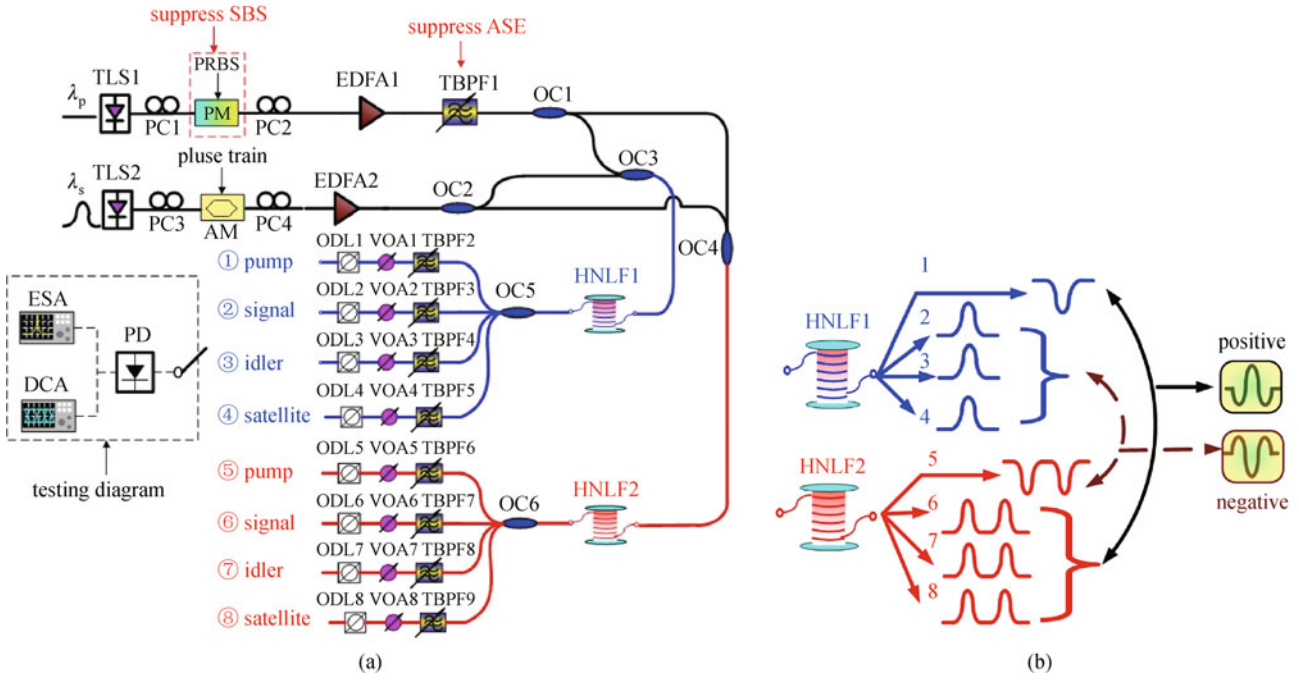

Fig. 1 (a) Parallel FOPA configuration; (b) schematic diagram of polarity-inverted UWB doublets generation process. PCs: polarization controllers; OCs(1–4): 1/1 optical couplers; OCs(5,6): 1/4 optical couplers; PM: phase modulator; PD: photodetector

amplified in the line-gain regime with its temporal-profile holding, while in the gain-saturation regime, it splits up into two sub pulses, is emphasized in Refs. [9,10]. In terms of this, Fig. 2 illustrates the temporal profiles the signal, pump, idler and satellite waves (blue line for a 250-m fiber and red line for a 450-m fiber). For HNLF1, since the FOPA operates in a line-gain regime, the signal pulse is linearly amplified without distortion, and simultaneously, the idler and satellite waves duplicate the information of the signal wave with the result of an overshoot generated, while the pump wave with an undershoot is formed, owing to the optical-parametric-attenuation effect. As for HNLF2, because a strong-strength interaction among waves takes place, the FOPA works in a gain-saturation mode, accompanied with the signal wave splitting up into two sub pulses, and the waveforms of the idler and satellite are approximately identical to that of the signal. Meanwhile, the pump wave with a double-undershoot is also obtained, as analyzed in the preceding. The pulse durations for the overshoot or the undershoot are indicated in Fig. 2, which are slightly different among them, maybe resulted from the gain-competition and different phase-matching conditions in the multiple four-wave mixing processes [12,13].

Figure 3 displays 6-channel polarity-inverted UWB doublets together with their corresponding spectral intensities, under the condition of different relative time advance/delays (RTADs) between the overshoot and the undershoot. Figures 3(a)–3(c) show temporal profiles for the positive UWB_{25}, UWB_{35}, and UWB_{45} doublets, while

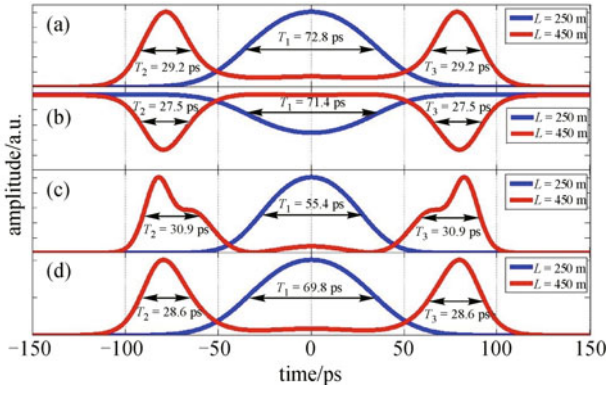

Fig. 2 Temporal waveforms for (a) signal; (b) pump; (c) idler; (d) satellite waves with fiber lengths of 250 and 450 m, respectively

their corresponding spectral intensities are illustrated in Figs. 3(d)–3(f). Remarkably, when the overshoot is deviated from the central location for a certain distance (i.e., shift toward the negative direction of time axis), as seen in Figs. 3(b) and 3(c) with RTADs of $\Delta T_1 = 5$ ps and $\Delta T_2 = 10$ ps, the generated UWB doublets are not symmetric with respect to the center point, but their spectral intensities also satisfy the requirement of FCC regulation (see Figs. 3(e) and 3(f)), i.e., the key parameters for the UWB_{45} doublet are Fc = 5.79 GHz, BW_{10dB} = 8.58 GHz and FBW = 148.19%. Similarly, the negative UWB_{16},

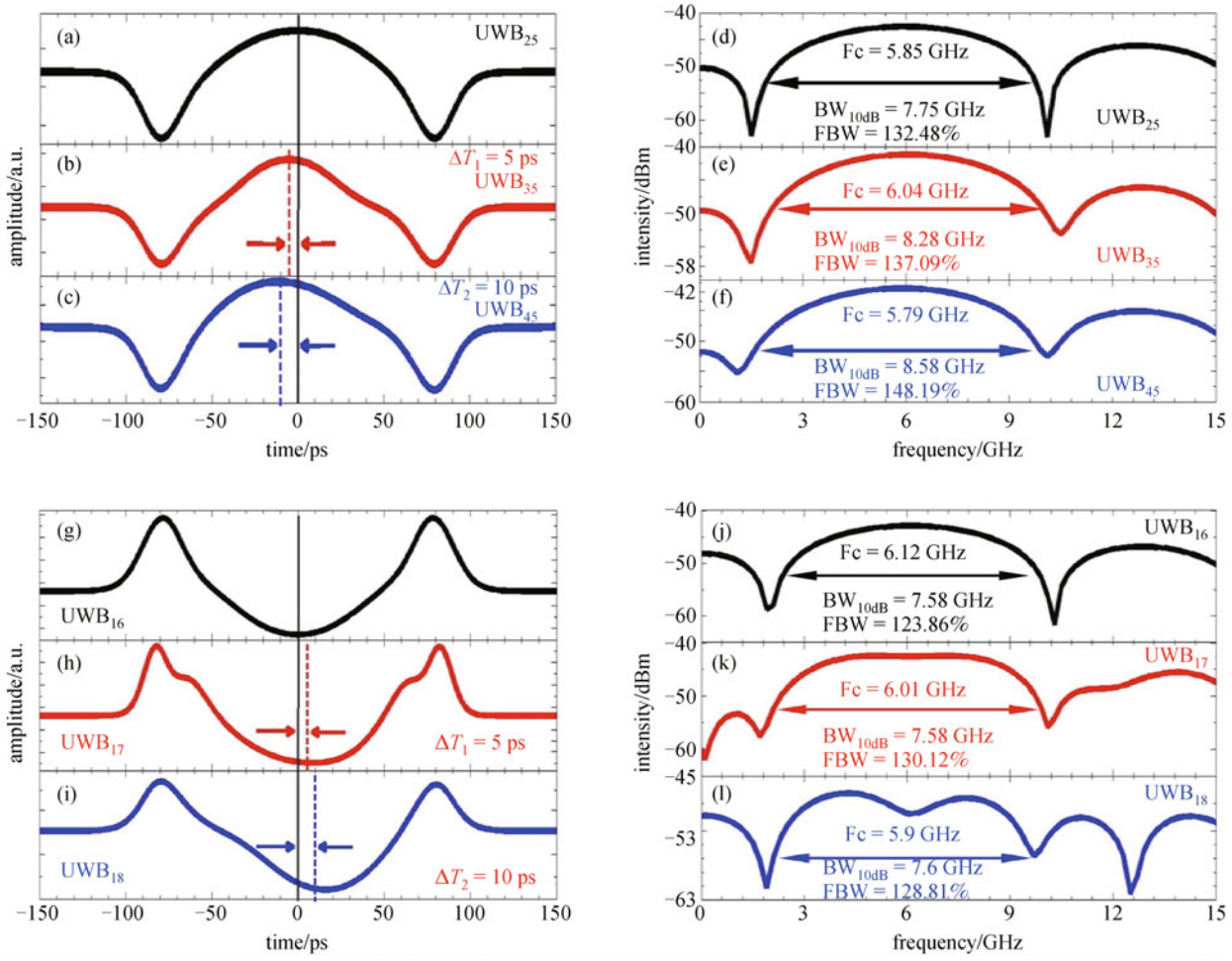

Fig. 3 Temporal and spectral intensity for positive and negative UWB doublet for different channels with different RTADs

UWB_{17}, and UWB_{18} doublets are also illustrated with the undershoot shifting toward the positive direction of time axis, as seen in Figs. 3(h) and 3(i). Likewise, we note that the RTADs in Figs. 3(h) and 3(i) are $\Delta T_1 = 5$ ps and $\Delta T_2 = 10$ ps, respectively, and the corresponding temporal profiles for UWB doublets are distorted to a certain extent, compared to Fig. 3(g) without RTAD. From the view of the spectral intensity, however, the UWB doublets in Figs. 3(h) and 3(i) both satisfy the FCC regulation, i.e., the key parameters for the UWB_{18} doublet are Fc = 5.9 GHz, BW_{10dB} = 7.6 GHz and FBW = 128.81%. Therefore, our scheme for the generation of UWB-doublet has good tolerance to the RTAD.

Ulteriorly, we discuss how the duration of the initial Gaussian signal influences the UWB doublet waveform, and Figs. 4(a)–4(c) illustrate the temporal profiles for the negative UWB_{16} doublet with different signal durations of $T_{01} = 30$, $T_{02} = 35$ and $T_{03} = 40$ ps, respectively, from which it can be clearly seen that, the pulse duration of a UWB doublet is broadened with the increase of the pulse duration of the initial Gaussian signal in temporal domain, resulting in compression in the spectral domain for the UWB doublet. For example, BW_{10dB} of the UWB_{16} doublet marked with blue line in Fig. 4(d), corresponding to $T_{03} = 40$ ps, is much narrower than that marked with red line, corresponding to $T_{01} = 30$ ps. This interesting finding can be potentially utilized to the UWB waveform optimization.

3 Conclusions and discussion

In summary, we propose a parallel FOPA structure to realize the generation of 6-channel polarity-inverted UWB doublets by exploiting the gain-saturation and optical-parametric-attenuation effects in HNLF. The key devices in our scheme are two pieces of HNLFs with fiber lengths of 250 and 450 m, respectively, which make the parallel FOPA configuration operate simultaneously in the linear-gain and gain-saturation modes in different optical fibers, resulting in the formation of the single- or double-overshoot and undershoot. The temporal and spectral

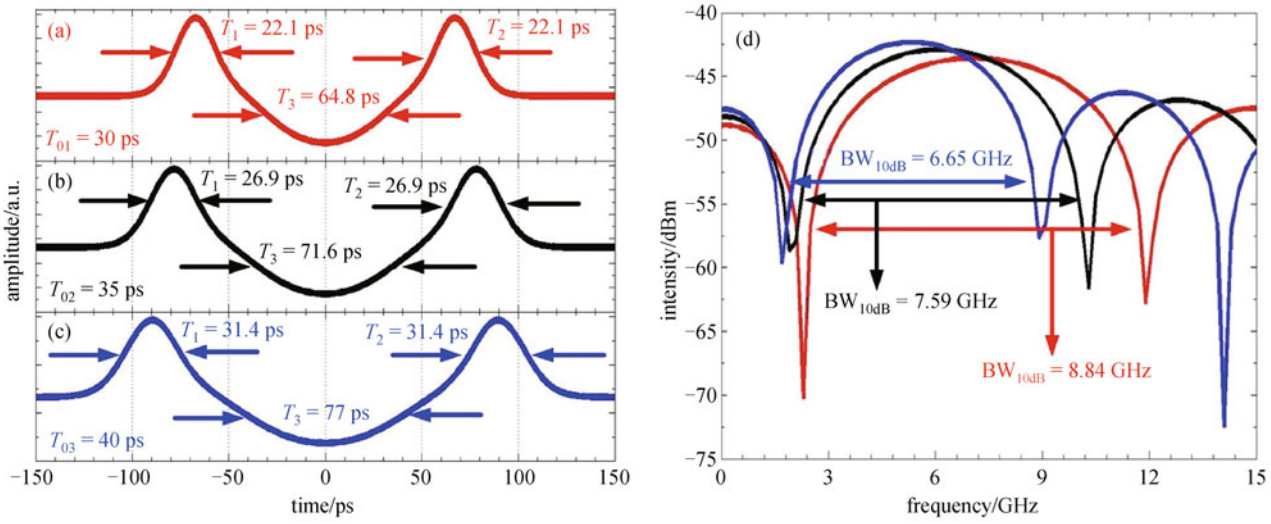

Fig. 4 Temporal profiles ((a), (b), and (c)) and corresponding spectral intensities (d) for the UWB_{16} doublet with different initial signal pulse durations

intensities for 6-channel UWB doublets are investigated with a proper selection of the RTAD, and one can find that our scheme has good tolerance to the RTAD. Finally, we optimize the UWB doublet by properly selecting the initial signal duration, and all the UWB doublets obtained from our proposal meet the FCC regulation.

However, the spectral intensity for the UWB doublet cannot exactly match with the FCC mask, due to the high-frequency components exceeding the limit of the FCC mask, but this does not impact much on the UWB-over-fiber communication, for it can be easily solved from the following three aspects: (1) we can artificially select a proper fiber length, assisted with tuning the strength of the overshoot or the undershoot of a UWB doublet [10]; (2) the UWB-over-fiber technology can be utilized to eliminate the unnecessary high-frequency components [10]; (3) the UWB antenna [14] with band-pass characteristics can be adopted to shape the spectra of the radiated pulses under specific emission limits within allowed frequency ranges (3.1–10.6 GHz). In addition, although the higher-order UWB pulse (i.e., UWB triplet pulse) can best meet the FCC mask, it is at the expense of the cost and is detrimental to modulation.

Acknowledgements This work was supported by the National Natural Science Foundation of China (Grant No. 60977044). The authors acknowledge the helpful discussions with Jing Shao, Jinqiang Zeng and Kang Tan in our team.

References

1. McKinney J D, Lin I S, Weiner A M. Shaping the power spectrum of ultra-wideband radio-frequency signals. IEEE Transactions on Microwave Theory and Techniques, 2006, 54(12): 4247–4255
2. Yang L Q, Giannakis G B. Ultra-wideband communications: an idea whose time has come. IEEE Signal Processing Magazine, 2004, 21 (6): 26–54
3. Yao J P. Photonic generation of microwave arbitrary waveforms. Optics Communications, 2011, 284(15): 3723–3736
4. Zhang Y, Zhang X L, Zhang F Z, Wu J, Wang G H, Shum P P. Photonic generation of millimeter-wave ultra-wideband signal using microfiber ring resonator. Optics Communications, 2011, 284(7): 1803–1806
5. Yao J P, Zeng F, Wang Q. Photonic generation of ultrawideband signals. IEEE Photonics Technology Letters, 2007, 25(11): 3219–3235
6. Wang J, Sun Q Z, Sun J Q, Zhang W W. All-optical UWB pulse generation using sum-frequency generation in a PPLN waveguide. Optics Express, 2009, 17(5): 3521–3530
7. Bolea M, Mora J, Ortega B, Capmany J. Optical UWB pulse generator using an *N* tap microwave photonic filter and phase inversion adaptable to different pulse modulation formats. Optics Express, 2009, 17(7): 5023–5032
8. Li Z L, Lai P T, Choi H W. A reliability study on green InGaN–GaN light-emitting diodes. IEEE Photonics Technology Letters, 2009, 21 (19): 1429–1431
9. Cao H, Sun J Q, Huang D X. Unique dispersion effects on transmitting and amplifying of picosecond pulses in fiber optical parametric amplifiers. Proceedings of SPIE, 2005, 6019: 601931-1–601931-9
10. Zhao L, Sun J Q, Huang D X. Photonic generation of ultrawideband signals by exploiting gain saturation of dark pump pulse with double undershoots in a highly nonlinear fiber. Optics Communications, 2011, 284(6): 1669–1676
11. Zhao L, Sun J. Investigation of the phase-locking behavior by utilizing self-phase- and cross-phase-modulation in cubic susceptibility medium: theory and experiment. Physical Review A, 2010, 82(6): 063831

12. Liu X M. Theory and experiments for multiple four-wave-mixing processes with multifrequency pumps in optical fibers. Physical Review A, 2008, 77(4): 043818
13. Liu X M, Zhou X Q, Lu C. Multiple four-wave mixing self-stability in optical fibers. Physical Review A, 2005, 72(1): 013811
14. Lin W P, Li R C. Generation of ultrawideband pulses using a distributed fiber-link system. Optical Fiber Technology, 2008, 14(3): 214–221